JOURNAL OF BONE AND MINERAL RESEARCH
Volume 24, Number 6, 2009
Published online on December 29, 2008; doi: 10.1359/JBMR.081255

Bone Structure at the Distal Radius During Adolescent Growth

Salman Kirmani,[1,2] David Christen,[2,3] G. Harry van Lenthe,[3] Philip R. Fischer,[1] Mary L. Bouxsein,[4] Louise K. McCready,[1] L. Joseph Melton III,[1] B. Lawrence Riggs,[1] Shreyasee Amin,[1] Ralph Müller,[3] and Sundeep Khosla[1]

ABSTRACT: The incidence of distal forearm fractures peaks during the adolescent growth spurt, but the structural basis for this is unclear. Thus, we studied healthy 6- to 21-yr-old girls (n = 66) and boys (n = 61) using high-resolution pQCT (voxel size, 82 μm) at the distal radius. Subjects were classified into five groups by bone-age: group I (prepuberty, 6–8 yr), group II (early puberty, 9–11 yr), group III (midpuberty, 12–14 yr), group IV (late puberty, 15–17 yr), and group V (postpuberty, 18–21 yr). Compared with group I, trabecular parameters (bone volume fraction, trabecular number, and thickness) did not change in girls but increased in boys from late puberty onward. Cortical thickness and density decreased from pre- to midpuberty in girls but were unchanged in boys, before rising to higher levels at the end of puberty in both sexes. Total bone strength, assessed using microfinite element models, increased linearly across bone age groups in both sexes, with boys showing greater bone strength than girls after midpuberty. The proportion of load borne by cortical bone, and the ratio of cortical to trabecular bone volume, decreased transiently during mid- to late puberty in both sexes, with apparent cortical porosity peaking during this time. This mirrors the incidence of distal forearm fractures in prior studies. We conclude that regional deficits in cortical bone may underlie the adolescent peak in forearm fractures. Whether these deficits are more severe in children who sustain forearm fractures or persist into later life warrants further study.
J Bone Miner Res 2009;24:1033–1042. Published online on December 29, 2008; doi: 10.1359/JBMR.081255

Key words: adolescent, BMD, BMC, pQCT

Address correspondence to: *Sundeep Khosla, MD, Endocrine Research Unit, Guggenheim 7-11A, Mayo Clinic, 200 First Street SW, Rochester, MN 55905, USA, E-mail: khosla.sundeep@mayo.edu*

INTRODUCTION

The most common site of fracture during adolescence is the distal forearm, and the incidence peaks at the time of the pubertal growth spurt.[1–3] The incidence of forearm fractures in childhood is rising,[1–4] and our previous study in Rochester, MN, showed that forearm fractures have increased by 32% in boys and 56% in girls over the past 30 yr.[5] Changes in recreational activities and participation in sports seem to account for only part of the increased incidence of these fractures,[5] raising the possibility that the acquisition of bone mass (and thus bone strength) during adolescence is being impaired. Whether this is caused by changing dietary habits or other lifestyle factors is not clear. Nonetheless, because 25–50% of the peak bone mass of adulthood is accumulated during the pubertal growth spurt,[6] it is possible that adolescents today will be at increased risk for osteoporotic fractures later in life.[7]

Previous studies using DXA have found significant increases in bone mass through puberty,[8,9] but size-corrected DXA measurements suggest decreases in areal BMD (aBMD) during peak linear growth.[10] Studies using pQCT at the distal radius found no changes in trabecular volumetric BMD (vBMD), but increases in cortical vBMD toward the end of puberty.[11,12] Decreased aBMD[13–15] and bone cross-sectional area[11,16,17] have also been found at the ultradistal radius in children with forearm fractures compared with control children. However, these studies are limited by the imaging techniques used: DXA measurements are confounded by bone size and are unable to differentiate cortical from trabecular bone. The standard pQCT used in previous studies in children has a resolution of ~400 μm and thus lacks the ability to accurately assess bone microarchitecture or to evaluate bone strength. This is now possible using high-resolution pQCT (HRpQCT), which has a voxel size of 82 μm, can define trabecular and cortical microstructure, shows excellent correlation with ex vivo μCT imaging (resolution of 20 μm or better),[18,19] and can be used to construct microfinite element (μFE) models of bone strength.[20] We recently used this technique in adults to obtain an in vivo assessment of bone microarchitecture across life in women and men, making it possible to obtain ''noninvasive bone biopsy''[21] data in population studies.[22] Because of its high resolution, this

The authors state that they have no conflicts of interest.

[1]College of Medicine, Mayo Clinic, Rochester, Minnesota, USA; [2]These authors contributed equally to this work; [3]Institute for Biomechanics, ETH Zürich, Zürich, Switzerland; [4]Orthopedic Biomechanics Laboratory, Beth Israel Deaconess Medical Center and Harvard Medical School, Boston, Massachusetts, USA.

technique allows for the study of microarchitectural changes in bone during growth in humans. We thus conducted a cross-sectional study to quantify changes in bone microarchitecture and strength at the distal radius in girls and boys through puberty, specifically testing the hypothesis that changes in bone microarchitecture during this period may provide an explanation for the observed peak in the incidence of forearm fractures in adolescence.[1–3] We further measured a number of key biochemical and hormonal parameters and related these to the observed microarchitectural and strength variables to define potential determinants of these variables during growth.

MATERIALS AND METHODS

Study subjects

The study was approved by the Mayo Clinic Institutional Review Board. Informed written consent was obtained from all subjects >12 yr of age and from a parent for all subjects <18 yr of age. We recruited 140 healthy girls and boys ($n = 70$ for each sex) age 6–21 yr without prior history of fracture. Reflecting the ethnic composition of the population of Rochester, MN, all but six subjects were white: four girls were black, one girl was white/Asian, and one boy was Asian. None of the subjects had a chronic illness, dietary restrictions, or intake of calcium supplements >1000 mg/d or vitamin D supplements >200 IU/d. No subject had ever used sodium fluoride, calcitonin, bisphosphonates, antiepileptic drugs, or had a history of oral steroid use for >7 days. None of the girls had a history of oral contraceptive use. Skeletal maturity was assessed using plain hand and wrist X-rays, and subjects were divided into groups based on bone-age using the Tanner-Whitehouse III method,[23] although subjects who had completed skeletal maturation (bone-age >15 yr for girls and >16.5 yr for boys) were classified according to chronological age. We divided the subjects into five groups: group I, prepubertal (bone-age 6–8 yr); group II, early pubertal (bone-age 9–11 yr); group III, midpubertal (bone-age 12–14 yr); group IV, late pubertal (bone-age 15–17 yr); and group V, postpubertal (age 18–21 yr). Anthropometric data were collected on all subjects. Calcium and vitamin D intake was assessed using a 3-day food diary, as previously described.[24,25] All subjects underwent a physical examination for pubertal Tanner stage assessment. Data on 13 subjects were excluded because of motion artifact in the HRpQCT scans; thus, 127 subjects (66 girls and 61 boys) were analyzed.

HRpQCT measurements

Measurements were obtained from the nondominant wrist on all subjects using the Xtreme CT (Scanco Medical, Brüttisellen, Switzerland). Using a scout view, a reference line was set at the proximal limit of the epiphyseal growth plate. For subjects whose epiphyseal plates had fused, the remnant of the plate was still visible to set the reference line. The scan was performed on a segment spanning 9.02 mm, starting at a distance 1 mm proximal to the reference line, thereby ensuring that, despite differences in arm length, all subjects had the scans performed as close to the identical anatomic site as possible; this is also the site where adolescent fractures most commonly occur.[1–3] Data were obtained using a 3D stack of 110 high-resolution CT slices with an isotropic voxel size and slice thickness of 82 μm, using an effective energy of 40 keV, field of view of 125.9 mm, and image matrix of 1536 × 1536 pixels. The radiation exposure to the subjects was minimal (local absorbed dose, 0.065 cGy; total radiation exposure, <0.01 mSv).

Trabecular parameters: Bone volume/total volume (BV/TV, %) was derived from trabecular vBMD, assuming mineral density of fully mineralized bone of 1.2 g hydroxyappatite/cm^3. Recognizing that individual trabeculae would not be resolved at their correct thickness (~100 μm) because of partial volume effects, a thickness-independent structure extraction was used to identify 3D ridges (center points of the trabeculae)[26]; trabecular number (Tb.N, mm^{-1}) was taken as the inverse of the mean spacing of the ridges.[27] Analogous with standard histomorphometry,[28] trabecular thickness (Tb.Th, μm) was calculated using the formula, Tb.Th = BV/TV ÷ Tb.N, and trabecular spacing (Tb.Sp, μm) was calculated as Tb.Sp = (1 − BV/TV) ÷ Tb.N. Validation studies show excellent correlation ($R \geq 0.96$) for these parameters compared with the gold standard ex-vivo μCT technique.[18]

Cortical parameters: The cortex was segmented from the grayscale image with a Gaussian filter and threshold.[27] Cortical vBMD and area were measured directly, and the periosteal circumference was calculated from the contour. Cortical thickness (Ct.Th, μm) was derived using the following formula: Ct.Th = area/circumference. Again, excellent correlation ($R = 0.98$) has been shown for Ct.Th measurements with HRpQCT versus μCT.[19] Endocortical circumference was calculated assuming that the trabecular compartment was circular. The automatically generated cortical mask was applied to the whole bone structure to obtain the cortical bone, followed by an inversion resulting in a negative image, including only the ''cortical pores.'' The cortical porosity index was defined as the ratio of cortical pore volume to cortical bone volume.

μFE analysis: Bone strength at the ultra-distal radius was calculated directly from μFE models.[29] Conceptually, a complicated object is divided into a finite number of small and manageable pieces (i.e., elements), using a direct conversion of voxels to hexahedral elements. Frictionless plate compression testing of the region as assessed by HRpQCT was simulated, with the material assumed to be isotropic and linear-elastic. A Young's modulus of 10 GPa and a Poisson's ratio of 0.3[20,30] was applied. To solve these large problems with up to 16 million degrees of freedom, a PCG based parallel solver[31] was used on a CRAY XT4 system. Bone strength was estimated by scaling the resulting load from a test simulating 1% compression, such that 2% of all elements had an effective strain >7000 microstrain. Failure loads calculated from such μFE models correlated highly ($R = 0.87$) with compressive loads producing Colles' fractures in 54 cadaveric forearms.[20] Additionally, the relative load supported by cortical versus trabecular bone was assessed by calculating the strain energy dissipated in the cortex as a fraction of the total strain energy.

TABLE 1. Clinical, Anthropometric, and Biochemical Parameters in the Study Subjects

	Girls					Boys				
	I (6–8 yr)	II (9–11 yr)	III (12–14 yr)	IV (15–17 yr)	V (18–21 yr)	I (6–8 yr)	II (9–11 yr)	III (12–14 yr)	IV (15–17 yr)	V (18–21 yr)
N	11	17	16	13	9	7	16	13	16	9
Bone age (yr)	7.1 ± 0.2	10.0 ± 0.2	12.7 ± 0.2	15.3 ± 0.2	19.0 ± 0.3	7.1 ± 0.5	10.0 ± 0.2	13.4 ± 0.2	15.8 ± 0.2	19.2 ± 0.3
Chronological age (yr)	7.5 ± 0.3	10.3 ± 0.3	12.2 ± 0.2	15.3 ± 0.3	19.0 ± 0.3	7.6 ± 0.4	9.7 ± 0.4	13.4 ± 0.3	15.4 ± 0.5	19.5 ± 0.3
Tanner stage	1.1 ± 0.1	1.9 ± 0.2	3.4 ± 0.2	4.8 ± 0.1	5.0 ± 0.0	1.0 ± 0.0	1.5 ± 0.2	3.2 ± 0.2	4.7 ± 0.1	5.0 ± 0.0
Height (cm)	124 ± 1	143 ± 2*	156 ± 2*	164 ± 2*	165 ± 3*	130 ± 3	142 ± 2†	160 ± 2*	176 ± 2*‡	179 ± 2*§
Weight (kg)	24.7 ± 0.8	36.6 ± 1.6†	47.7 ± 1.7*	63.3 ± 3.3*	66.6 ± 5.2†	28.6 ± 2.7	36.2 ± 2.2	51.7 ± 2.5*	69.7 ± 2.7*	74.4 ± 3.2*
BMI (kg/m^2)	16.0 ± 0.3	17.9 ± 0.8	19.6 ± 0.8**	23.5 ± 1.2*	24.2 ± 1.7*	16.9 ± 1.2	17.8 ± 0.7	20.2 ± 0.8	22.6 ± 1.0*	23.2 ± 0.9*
Calcium intake (mg/d)	1013 ± 140	1222 ± 161	1112 ± 109	1223 ± 161	814 ± 208	1123 ± 260	1210 ± 98	1423 ± 176	1609 ± 163	1178 ± 464
Vitamin D intake (IU/d)	212 ± 41	225 ± 33	223 ± 30	236 ± 42	184 ± 82	246 ± 5	225 ± 21	257 ± 41	330 ± 64	258 ± 146
PINP (μg/liter)	273 ± 5	275 ± 9	263 ± 8	143 ± 15*	89.1 ± 8*	295 ± 13	311 ± 10§	319 ± 11‡	251 ± 14‡	124 ± 10*§
CTX (ng/ml)	2.3 ± 0.1	2.2 ± 0.1	2.3 ± 0.2	1.1 ± 0.1*	0.8 ± 0.1*	1.9 ± 0.2	1.8 ± 0.2§	2.4 ± 0.2	1.8 ± 0.2§	1.2 ± 0.1
25(OH)D (ng/ml)	25.5 ± 1.8	23.9 ± 1.4	19.9 ± 0.9**	22.4 ± 1.6	22.1 ± 1.9	31.2 ± 4.0	30.8 ± 1.3‡	26.8 ± 1.2‡	27.9 ± 2.0§	29.2 ± 2.8
PTH (pg/ml)	30.8 ± 3.5	24.6 ± 2.0	38.8 ± 4.2	29.4 ± 4.6	28.4 ± 3.5	37.2 ± 2.9	26.7 ± 3.3	36.8 ± 4.3	36.4 ± 6.2	24.7 ± 3.5
E_2 (pg/ml)	2.0 ± 0.5	8.9 ± 2.5	49.3 ± 7.0	104 ± 18.9*	126 ± 33.8*	0.0 ± 0.0§	0.7 ± 0.2§	7.4 ± 1.5‡	23.1 ± 1.9*‡	29.1 ± 8.8*§
T (ng/dl)	4.2 ± 0.6	9.3 ± 0.9	23.6 ± 2.4*	33.5 ± 3.2*	36.1 ± 3.9*	2.6 ± 0.7	16.2 ± 8.6	220 ± 52†‡	584 ± 34*‡	510 ± 28*‡
IGF-I (ng/ml)	160 ± 22	294 ± 38	705 ± 74*	601 ± 32*	425 ± 45**	213 ± 57	246 ± 22	529 ± 42*	624 ± 41*	354 ± 27
IGFBP-2 (ng/ml)	603 ± 114	415 ± 36**	372 ± 35**	294 ± 35†	424 ± 95	545 ± 211	505 ± 60	445 ± 58	469 ± 58§	493 ± 72
IGFBP-3 (μg/ml)	3.6 ± 0.16	4.6 ± 0.19**	5.5 ± 0.23*	5.2 ± 0.14*	4.7 ± 0.22**	4.0 ± 0.30	4.4 ± 0.16	5.4 ± 0.20*	5.2 ± 0.14†	4.9 ± 0.25**

All data expressed as means ± SE. Group V was classified according to chronological age, because they had attained full skeletal maturity.

* $p < 0.001$ † $p < 0.01$, and ** $p < 0.05$ vs. group I.

‡ $p < 0.001$, § $p < 0.01$, and ¶ $p < 0.05$ for comparison with the respective group of girls.

BMI, body mass index; PINP, amino-terminal propeptide of type I collagen; CTX, C-terminal telopeptide of type I collagen; 25(OH)D, 25-hydroxyvitamin D; E_2, estradiol; T, testosterone.

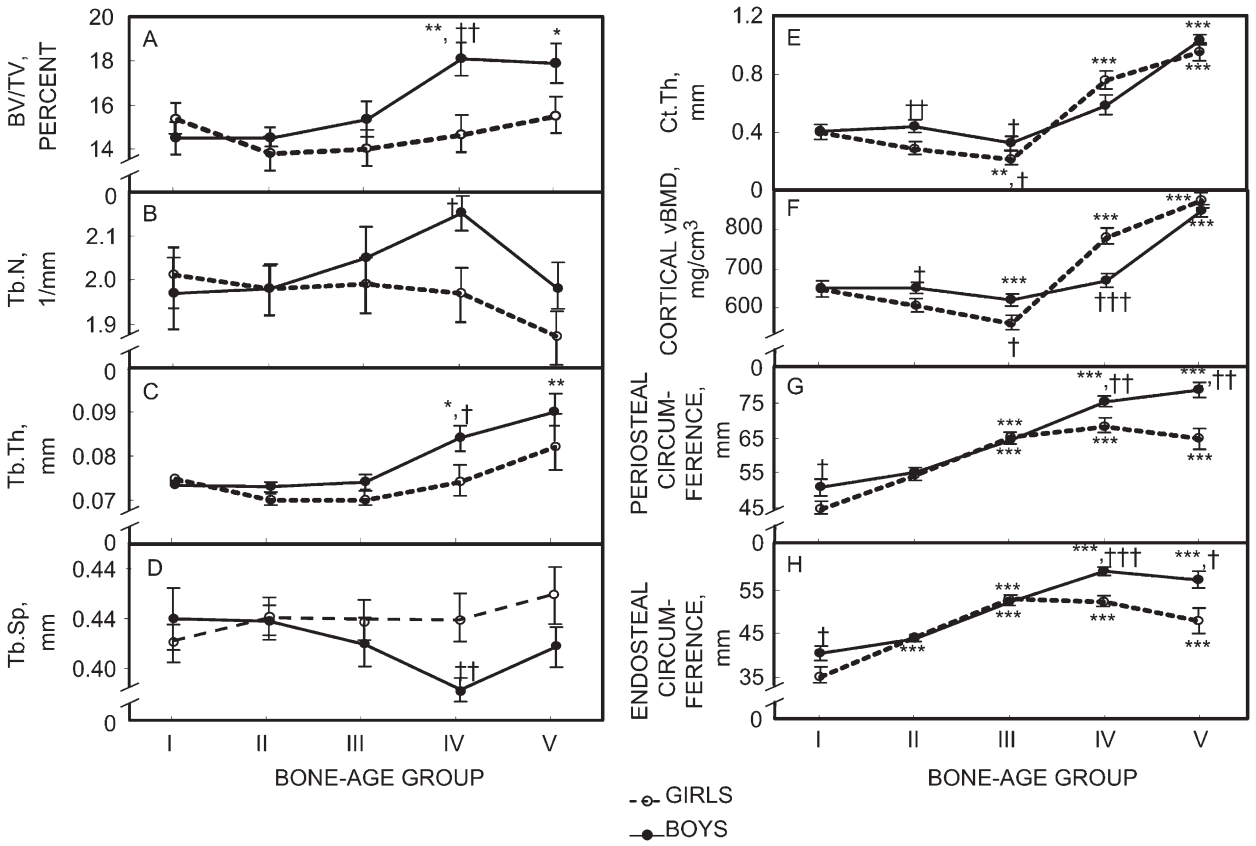

FIG. 1. Trabecular and cortical bone parameters in bone-age groups I through V. (A) BV/TV, bone volume/total volume; (B) Tb.N, trabecular number; (C) Tb.Th, trabecular thickness; (D) Tb.Sp, trabecular spacing; (E) Ct.Th, cortical thickness; (F) cortical vBMD; (G) periosteal circumference; (H) endosteal circumference. $^{*}p < 0.05$, $^{**}p < 0.01$, and $^{***}p < 0.001$ vs. group I; $^{\dagger}p < 0.05$, $^{\dagger\dagger}p < 0.01$, and $^{\dagger\dagger\dagger}p < 0.001$ for comparison with the respective group of girls.

Applied loads and factor-of-risk

For these estimates, we used the loading conditions for a forward fall. The load applied to the wrist was estimated from predicted impact forces on the upper extremity during a fall on the outstretched hand.[32] We assessed the ratio of fall load to overall bone strength, as determined by μFE, as an estimate of the load-to-strength ratio, or factor of risk (Φ).

Areal BMD, BMC, and bone area measurements

aBMD, BMC, and bone area measurements were made from DXA scans performed on the nondominant radius (total radius) (Lunar Prodigy System; GE Healthcare, Madison, WI, USA).

Hormone and bone turnover measurements

A serum bone formation marker, amino-terminal propeptide of type I collagen (PINP), and a serum bone resorption marker, C-terminal telopeptide of type I collagen (CTX), were measured using ELISAs (Immunodiagnostic Systems, Fountain Hills, AZ, USA, for PINP [intra-assay CV < 10%] and Nordic Biosciences, Herlev, Denmark, for CTX [CV < 8%]). IGF-1 and IGFBP-2 were measured by radioimmunoassay (Diagnostic Systems Laboratories, Webster, TX, USA; CVs < 7%). IGFBP-3 was measured by immunoradiometric assay (Diagnostic Systems Laboratories; CV = 3%). PTH was measured by automated immunometric assay (Diagnostic Products, Los Angeles, CA, USA; CV = 7%), and 25-hydroxyvitamin-D [25(OH)D], total estradiol (E_2), and testosterone (T) were measured using tandem mass spectroscopy (API 5000; Applied Biosystems-MDS Sciex, Foster City, CA, USA). Details regarding the mass spectroscopy measurements have been previously described.[33]

Statistical analysis

Data are expressed as means ± SE. For all parameters, the mean values of each bone-age group were compared using one-way ANOVA and compared with the prepubertal bone-age group (group I, 6–8 yr) using Dunnet's test, accounting for multiple comparisons. This analysis was performed using the entire cohort as well as excluding the six nonwhite subjects (see above); however, because the pattern of differences in all variables across pubertal groups was virtually identical with or without inclusion of the nonwhite subjects, the data presented are those including all subjects. Associations between imaging parameters and serum biochemical/hormonal variables were

assessed using multivariable linear regression models. On these models, both bone age and bone age^2 were used, because some of the observed relationships were nonlinear. A stepwise variable selection process was used to build the models.

RESULTS

Table 1 shows the clinical, anthropometric, and hormonal/biochemical parameters in the study subjects. As is evident, in this healthy cohort of children, bone age corresponded closely to chronological age. Tanner stages advanced as expected with bone age. Boys were taller than girls in late puberty, but weight and BMI were similar. Calcium and vitamin D intake were also similar in girls and boys and did not differ significantly across bone age groups. Serum PINP levels were higher in boys than girls by early puberty (group II) and remained significantly higher in the boys thereafter. Both serum PINP and CTX levels tended to be lower in girls and boys in the late pubertal groups. Serum 25(OH)D levels were higher in all groups in boys, reaching statistical significance in groups II, III, and IV. Serum PTH levels were similar across all groups and did not differ between sexes. Serum sex steroid and IGF-I levels showed the expected changes during adolescence. Serum IGFBP-2 levels tended to be lower through puberty and be higher in boys compared with girls, whereas serum IGFBP-3 levels changed in parallel with serum IGF-I levels, reflecting increases in growth hormone secretion.

Figure 1 shows the trabecular and cortical structural parameters from the HRpQCT scans. Compared with the prepubertal group (group I), girls showed no significant difference in BV/TV, Tb.N, Tb.Th, or Tb.Sp through puberty, whereas boys showed significant increases in BV/TV, and Tb.Th in late to postpuberty. Compared with girls, boys had significantly higher values for BV/TV and Tb.Th, but not Tb.N, from late puberty onward. Girls showed significant decreases in Ct.Th and cortical vBMD in midpuberty before increasing sharply at the end of puberty. Conversely, boys maintained Ct.Th and cortical vBMD from pre- to midpuberty, before showing marked increases toward the end of puberty. There was no difference in Ct.Th or cortical vBMD between boys and girls at the end of puberty. In both sexes, periosteal and endosteal circumference by HRpQCT rose from pre- to midpuberty, coming to a plateau toward the end of puberty. In contrast to these structural changes defined by HRpQCT, aBMD, BMC, and bone area by DXA at the total radius increased throughout puberty, with higher values in boys compared with girls at the end of puberty (Fig. 2).

Total bone strength, assessed using μFE models, was greater in both sexes from pre- to late puberty, reaching a plateau at the end of puberty in girls (Fig. 3A) but continuing to be higher even at the end of puberty in boys (Fig. 3B). Compared with girls, boys showed greater total bone strength after midpuberty. Because of the increase in height during growth, estimated fall force increased linearly in both sexes (Figs. 3C and 3D), but the load:strength ratio (factor-of-risk, Φ) decreased progressively during puberty in both girls and boys (Figs. 3E and 3F). Thus,

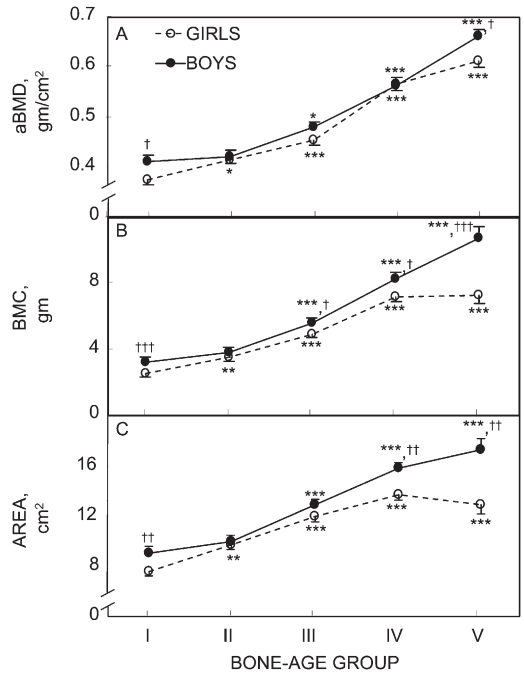

FIG. 2. DXA parameters at the radius in bone-age groups I through V. (A) aBMD, (B) BMC, and (C) bone area. *$p < 0.05$, **$p < 0.01$, and ***$p < 0.001$ vs. group I; $^{\dagger}p < 0.05$, $^{\dagger\dagger}p < 0.01$, and $^{\dagger\dagger\dagger}p < 0.001$ for comparison with the respective group of girls.

overall differences in bone strength, fall loads, or Φ could not provide a clear explanation for the midpubertal peak in distal forearm fractures. Further analysis of the μFE models showed, however, that during growth, the percent of load carried by cortical bone (Figs. 3G and 3H) and the ratio of cortical to trabecular bone volume (Figs. 3I and 3J) decreased sharply in midpuberty in both sexes, with these changes occurring around the ages of peak distal forearm fracture in adolescents.[1–3] Concurrently, the cortical porosity index also increased sharply in both sexes at these ages (Figs. 4A and 4B).

Figure 5 shows a visual representation of the changes in cortical and trabecular bone from subjects in the pre- (group I), mid- (group III), and postpubertal (group V) groups. The deficits in the cortical compartment in the midpubertal group are clearly evident in both sexes. In addition, Fig. 6 shows reconstructions of cortical bone from subjects in these groups, visually depicting the increase in cortical porosity during midpuberty.

Table 2 shows the results of the multivariate models for predicting the key bone structural and strength variables. None of the biochemical or hormonal variables were significantly associated with BV/TV, Tb.N, Tb.Th, or Tb.Sp in the girls, whereas greater BV/TV and Tb.Th were related to higher serum T levels and Tb.N and Tb.Sp were most closely associated with higher IGF-I levels in the boys. Ct.Th and cortical vBMD were inversely associated with the bone turnover markers in the girls and with PTH in the boys. Periosteal circumference was most closely associated with IGF-I levels in the girls and T levels in the boys; endosteal circumference was associated with IGF-I levels in

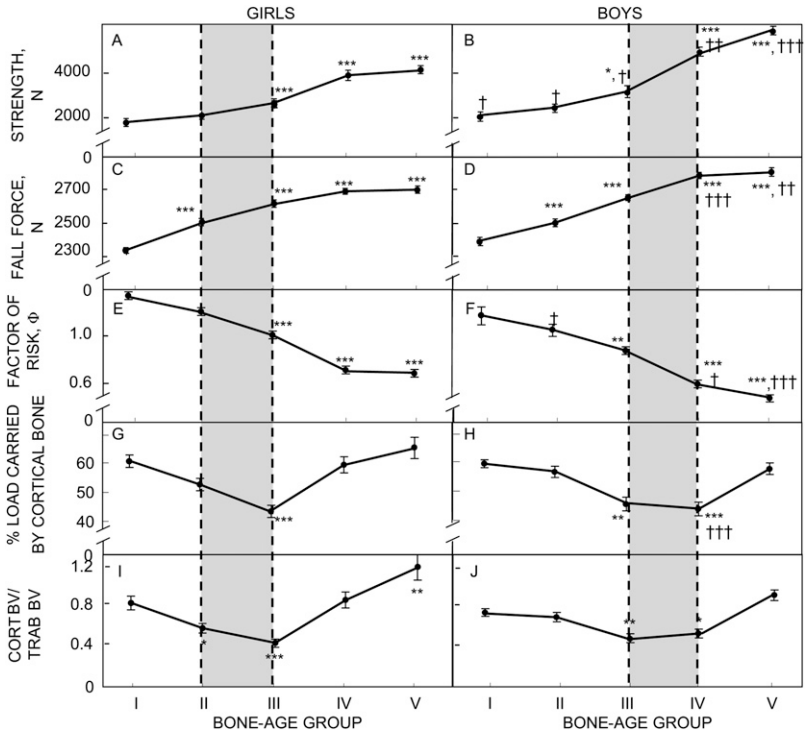

FIG. 3. (A and B) Total bone strength; (C and D) estimated fall loads; (E and F) factor of risk (Φ, ratio of fall loads to bone strength); (G and H) percent of load carried by cortical bone; and (I and J) ratio of cortical to trabecular bone volume in girls (left column) and boys (right column). Shaded regions represent the approximate chronological age ranges when the incidence of adolescent forearm fractures peaks based on previous data from Rochester, MN,[5] and elsewhere.[1–3] *$p < 0.05$, **$p < 0.01$, and ***$p < 0.001$ vs. group I; $^{\dagger}p < 0.05$, $^{\dagger\dagger}p < 0.01$, and $^{\dagger\dagger\dagger}p < 0.001$ for comparison with the respective group of girls.

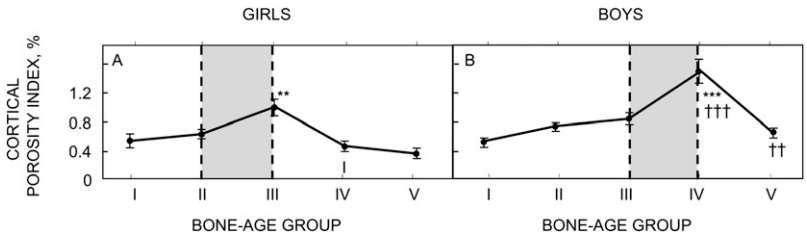

FIG. 4. Cortical porosity index in girls (A) and boys (B). Shaded regions represent the approximate chronological age ranges when the incidence of adolescent forearm fractures peaks based on previous data from Rochester, MN,[5] and elsewhere.[1–3] ***$p < 0.001$ vs. group I; $^{\dagger\dagger}p < 0.01$ and $^{\dagger\dagger\dagger}p < 0.001$ for comparison with the respective group of girls.

the girls and T levels in the boys. Overall bone strength was associated with serum E_2 levels in girls and T levels in boys. The percent load carried by cortical bone was negatively associated with CTX and IGF-I levels in the girls and negatively associated with IGF-I and PTH levels in the boys. The cortical porosity index, on the other hand, was positively associated with CTX and IGF-I levels in the girls and positively associated with IGF-I levels in the boys.

DISCUSSION

Combining HRpQCT with μFE analysis, we describe for the first time the changes that occur in bone microarchitecture and strength in healthy children during the course of puberty. We observed significant differences in trabecular and cortical bone development at the ultradistal radius between girls and boys during the pubertal growth spurt. Trabecular parameters did not change significantly during puberty in girls, suggesting that trabecular bone volume and structure at this site may be programmed early in life in girls and do not change significantly through growth. In contrast, trabecular BV/TV and Tb.Th were higher throughout puberty in boys, and these changes were driven mainly by T and IGF-1 levels. Changes in cortical bone also differed, with girls showing lower Ct.Th and cortical vBMD during midpuberty that was associated with elevated markers of bone turnover. Boys maintained Ct.Th and cortical vBMD through puberty; however, both parameters were negatively associated with PTH, suggesting that an increased demand for calcium during the more pronounced growth spurt in boys may be met by increasing PTH levels.[34] This may, in turn, compromise Ct.Th and cortical vBMD. The larger bone size, reflected by periosteal circumference, was driven mainly by T in boys and IGF-1 in girls, with boys showing a greater bone size from late puberty onward. Thus, whereas studies with estrogen receptor and aromatase-deficient men have clearly shown an important role for E in the development of the male skeleton,[35–39] our data suggest that T may regulate the development of trabecular structure and bone size in boys during puberty, although it remains possible that some of these effects of T may be mediated by local aromatization of T to E in bone.

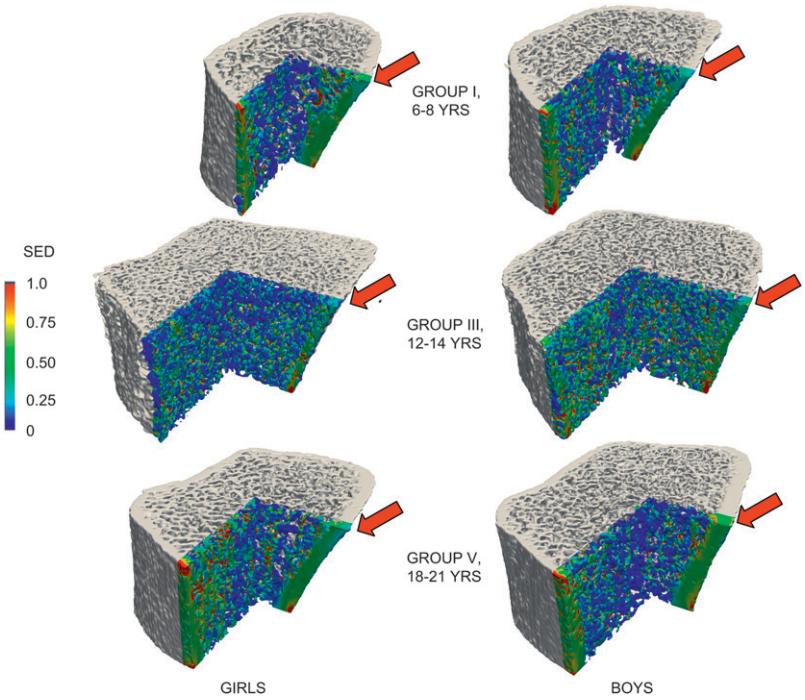

FIG. 5. Representative 3D reconstructions of trabecular and cortical bone of the measured region of the ultradistal radius in girls and boys from bone-age groups I, III, and V. The color coding is for the strain energy density (SED) from the μFE models, with low SED values indicating low strains (relatively strong areas) and high SED values indicating high strains (relatively weak areas). Note the thinning of the cortex (indicated by arrows) relative to the amount of trabecular bone present in the subjects in group III.

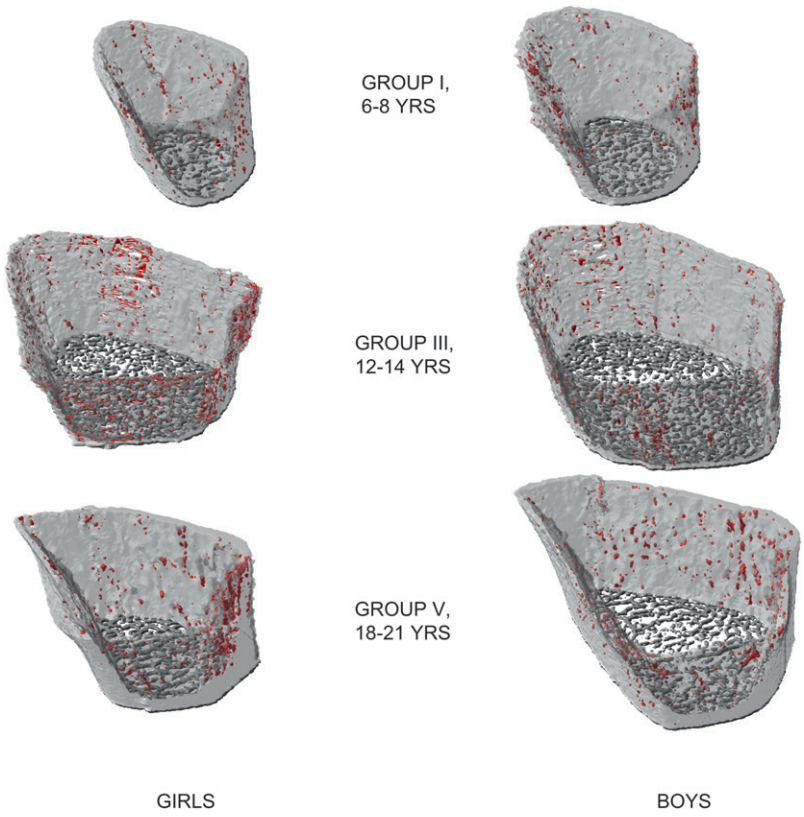

FIG. 6. Representative 3D reconstructions of cortical bone and the very proximal trabecular bone in girls and boys from bone-age groups I, III, and V. The areas in red indicate cortical pores used to calculate the cortical porosity index.

Our findings at the forearm are somewhat different from studies by Gilsanz et al.[40,41] using QCT at the spine and femur in growing children. Because of the lower resolution, those investigators could not assess bone structure, but they did observe increases in trabecular vBMD in late puberty in girls and boys. In addition, estimates of cortical vBMD at the midshaft of the femur showed little or no change during growth in girls or boys.[42] Whether

TABLE 2. Multivariable Models for the Key Bone Structural and Strength Variables in the Girls and Boys

	Girls				*Boys*			
Endpoints	*Predictors*	*Coefficient sign*	*p*	*Model adjusted R^2*	*Predictors*	*Coefficient sign*	*p*	*Model adjusted R^2*
BV/TV	—				T	Positive	<0.001	0.26
Tb.N	—				IGF1	Positive	0.014	0.09
Tb.Th	Bone age*	Negative	0.008	0.17	T	Positive	<0.001	0.28
	Bone age^2	Positive	0.003					
Tb.Sp	—				IGF-I†	Negative	0.006	0.11
C.Th	PINP	Negative	<0.001	0.70	Bone age	Negative	0.002	0.62
	CTX	Negative	0.004		Bone age^2	Positive	<0.001	
					PTH	Negative	0.001	
Cortical vBMD	PINP	Negative	<0.001	0.74	PINP	Negative	<0.001	0.62
	CTX	Negative	0.002		PTH	Negative	0.017	
Periosteal circumference	Bone age	Positive	<0.001	0.65	Bone age	Positive	<0.001	0.77
	Bone age^2	Negative	<0.001		T	Positive	0.008	
	IGF-I	Positive	0.033					
Endosteal circumference	Bone age	Positive	<0.001	0.57	Bone age	Positive	<0.001	0.68
	Bone age^2	Negative	<0.001		Bone age^2	Negative	0.009	
	IGF-I	Positive	0.047		PTH	Positive	0.006	
Strength	Bone age	Positive	<0.001	0.76	Bone age	Positive	<0.001	0.75
	BMI	Positive	0.004		T	Positive	0.013	
	E_2	Positive	0.032					
Φ (load/strength ratio)	Bone age	Negative	<0.001	0.72	Age	Negative	<0.001	0.75
	BMI	Negative	0.010		T	Negative	0.027	
Percent load carried by cortical bone	CTX	Negative	<0.001	0.40	IGF-I	Negative	<0.001	0.44
	IGF-I	Negative	0.003		PTH	Negative	<0.001	
Cortical porosity index	CTX‡	Positive	<0.001	0.31	IGF-I§	Positive	<0.001	0.22
	IGF-I	Positive	0.006					

Potential predictors included bone age, bone age^2, body mass index (BMI), amino-terminal propeptide of type I collagen (PINP), C-terminal telopeptide of type I collagen (CTX), 25(OH)D; PTH, estradiol (E_2), testosterone (T), IGF-I, IGF binding protein (IGFBP)-2, and IGFBP-3.

* Bone age, bone age^2, PINP, and E_2 were all close competitors as first variables of entry into the model.

† T was a close competitor as first variable of entry into the model.

‡ PINP was a close competitor as first variable of entry into the model.

§ T was a close competitor as first variable of entry into the model.

differences in trabecular and cortical bone changes between these central sites (vertebrae and femur) and the ultradistal radius site assessed in our study are caused by site-specific changes during growth, the particular techniques used (conventional QCT versus HRpQCT), or both is unclear and requires further study. Of note, previous studies using conventional pQCT at the forearm, while not able to assess bone structure, found similar changes in trabecular and cortical vBMD as described here.[11,12]

To try and explain the peak in forearm fracture risk during midpuberty,[1–3,5] we used μFE models to calculate bone strength during this key phase of growth. Total bone strength increased in both sexes through puberty, being driven mainly by T in boys and E_2 in girls, with a higher body mass index in girls being associated with greater bone strength. Boys showed greater bone strength than girls from late puberty onward, which continued to increase even at the end of puberty when growth was completed. However, changes either in bone strength or in the factor of risk failed to provide an explanation for the midpubertal increase in forearm fractures. Thus, it was of interest that the percent load borne by cortical bone (which reflects the relative strength of cortical to trabecular bone) and the cortical to trabecular bone volume ratio were at their lowest at midpuberty in girls and late puberty in boys, before rebounding to the original values seen at the start of puberty. This was accompanied by an increase in the cortical porosity index. These changes in cortical bone mirror the incidence of adolescent forearm fractures in a very similar population from Rochester[5] as well as other studies,[1–3] suggesting that these transient deficits in cortical bone during midpuberty may underlie the adolescent peak in forearm fractures. Of note, cadaveric studies have shown the importance of cortical bone as a critical determinant of failure load at the wrist,[43] and a similar reduction in the percent load borne by cortical bone has recently been reported in elderly women with wrist fractures.[44] Our in vivo estimates of cortical porosity are also consistent with the hypothesis proposed by Parfitt that transient increases in cortical porosity may develop in response to the increased calcium demand during rapid longitudinal growth.[34]

We should note that, in addition to analyzing our data using bone-age classifications, we also performed analyses using Tanner staging to classify the subjects and found that the pattern was essentially the same as was seen using bone-age assessments (data not shown). We specifically chose to classify subjects according to bone-age rather than Tanner stage for a number of reasons. First, we believe that bone-age gives a more accurate assessment of the effects

of sex steroids on skeletal maturity than Tanner staging. Bone-age assessment is the more objective of the two measures, thus making our classification more accurate. Also, if we restricted ourselves to Tanner stages, we would not be able to appreciate the changes that occur at the distal radius between late pubertal (age 15–17 yr) and postpubertal subjects (age 18–21 yr). As our data shows, there are significant differences in a number of measures during this time, and if all subjects between the ages of 15–21 yr were classified as one group, these differences would not be appreciated.

Our study has significant strengths and some potential limitations. Because of the high resolution possible with HRpQCT (voxel size, 82 μm), our data are perhaps at the limit of feasibility in terms of assessing bone microstructure in vivo in humans using a technology that has been validated for both trabecular and cortical parameters against the current gold standard, μCT (which can only be used in excised bones).[18,19] Nonetheless, we recognize that even with this high resolution, the parameters we assessed using HRpQCT are likely estimates of the true measures. In addition, our cross-sectional findings need to be confirmed by longitudinal studies, but it is important to note that these estimates seem to change in a predictable manner through puberty and reflect differences that have been observed in adults using bone biopsies. For example, our demonstration of a higher BV/TV and Tb.Th at the wrist toward the end of puberty in boys compared with girls is exactly what has been observed for differences in trabecular structure by histomorphometry in men versus women using iliac crest bone biopsies.[45] Thus, given limitations on radiation exposure, HRpQCT is perhaps the best validated tool to assess bone microstructure in humans, especially children.

In conclusion, our findings provide the first description of changes in bone structure during growth as well as a possible structural basis for the adolescent peak in forearm fractures. Further studies are needed to test whether the deficits in cortical bone we describe here are more severe in adolescents who sustain forearm fractures compared with control, nonfracture subjects. In addition, whether adults who sustained forearm fractures during adolescence have persistent skeletal deficits that may predispose them to osteoporotic fractures later in life also warrants further study.

ACKNOWLEDGMENTS

The authors thank Elizabeth Atkinson and Sara Achenbach for help with the statistical analyses, Kelley Hoey for sample processing, James Peterson for data management, Margaret Holets for performing the HRpQCT scans, and the Mayo Immunochemical Core Laboratory for performance of the biochemical and hormonal assays. We also thank the Data and Visualization group at the Swiss National Super Computing Centre CSCS for support. This work was supported in part by the Thrasher Research Fund, NIH Grants AR027065 and UL1-RR24150 (Center for Translational Science Activities), U.S. Public Health Service. Supercomputer time was granted by the Swiss National Supercomputing Centre (CSCS).

REFERENCES

1. Landin LA 1983 Fracture patterns in children. Acta Orthop Scand **54**(Suppl 202)**:**1–109.
2. Kramhoft M, Bodtker S 1988 Epidemiology of distal forearm fractures in Danish children. Acta Orthop Scand **59:**557–559.
3. Bailey DA, Wedge JH, McCulloch RG, Martin AD, Bernhardson SC 1989 Epidemiology of fractures of the distal end of the radius in children as associated with growth. J Bone Joint Surg Am **71:**1225–1231.
4. Tinkle BT, Wenstrup RJ 2005 A genetic approach to fracture epidemiology in childhood. Am J Med Genet C Semin Med Genet **139:**38–54.
5. Khosla S, Melton LJ III, Dekutoski MB, Achenbach SJ, Oberg AL, Riggs BL 2003 Incidence of childhood distal forearm fractures over 30 years: A population-based study. JAMA **290:**1479–1485.
6. Bailey DA, Martin AD, McKay HA, Whiting S, Mirwald R 2000 Calcium accretion in girls and boys during puberty: A longitudinal analysis. J Bone Miner Res **15:**2245–2250.
7. Hernandez CJ, Beaupré GS, Carter DR 2003 A theoretical analysis of the relative influences of peak BMD, age-related bone loss and menopause on the development of osteoporosis. Osteoporos Int **14:**843–847.
8. Kalkwarf HJ 2007 The bone mineral density in childhood study: Bone mineral content and density according to age, sex, and race. J Clin Endocrinol Metab **92:**2087–2099.
9. Cadogan J, Blumsohn A, Barker ME, Eastell R 1998 A longitudinal study of bone gain in pubertal girls: Anthropometric and biochemical correlates. J Bone Miner Res **13:**1602–1612.
10. Faulkner RA, Davison KS, Bailey DA, Mirwald RL, Baxter-Jones ADG 2006 Size-corrected BMD decreases during peak linear growth: Implications for fracture incidence during adolescence. J Bone Miner Res **21:**1864–1870.
11. Neu CM, Manz F, Rauch F, Merkel A, Schoenau E 2001 Bone densities and bone size at the distal radius in healthy children and adolescents: A study using peripheral quantitative computed tomography. Bone **28:**227–232.
12. Rauch F, Neu C, Manz F, Schoenau E 2001 The development of metaphyseal cortex–implications for distal radius fractures during growth. J Bone Miner Res **16:**1547–1555.
13. Goulding A, Cannan R, Williams SM, Gold EJ, Taylor RW, Lewis-Barned NJ 1998 Bone mineral density in girls with forearm fractures. J Bone Miner Res **13:**143–148.
14. Goulding A, Jones L, Taylor RW, Manning PJ, Williams SM 2000 More broken bones: A 4-year double cohort study of young girls with and without distal forearm fractures. J Bone Miner Res **15:**2011–2018.
15. Ma D, Jones G 2003 The association between bone mineral density, metacarpal morphometry, and upper limb fractures in children: A population-based case-control study. J Clin Endocrinol Metab **88:**1486–1491.
16. Binkley TL, Specker BL 2000 pQCT measurement of bone parameters in young children. J Clin Densitom **3:**9–14.
17. Moyer-Mileur L, Xie B, Ball S, Bainbridge C, Stadler D, Jee WSS 2001 Predictors of bone mass by peripheral quantitative computed tomography in early adolescent girls. J Clin Densitom **4:**313–323.
18. Laib A, Ruegsegger P 1999 Calibration of trabecular bone structure measurements of in vivo three-dimensional peripheral quantitative computed tomography with 28-micrometer-resolution microcomputed tomography. Bone **24:**35–39.
19. MacNeil JA, Boyd SK 2007 Accuracy of high-resolution peripheral quantitative computed tomography for measurement of bone quality. Med Eng Phys **29:**1096–1105.
20. Pistoia W, Van Rietbergen B, Lochmuller EM, Lill CA, Eckstein F, Ruegsegger P 2002 Estimation of distal radius failure load with micro-finite element analysis models based on three-dimensional peripheral quantitative computed tomography images. Bone **30:**842–848.
21. Muller R, Hildebrand T, Ruegsegger P 1994 Non-invasive bone biopsy: A new method to analyze and display the three-

dimensional structure of trabecular bone. Phys Med Biol **39:**145–164.
22. Khosla S, Melton LJ III, Achenbach SJ, Oberg AL, Riggs BL 2006 Hormonal and biochemical determinants of trabecular microstructure at the ultradistal radius in women and men. J Clin Endocrinol Metab **91:**885–891.
23. Tanner JM, Healy MJR, Goldstein H, Cameron N 2001 Assessment of Skeletal Maturity and Prediction of Adult Height: TW3 Method. Saunders, Philadelphia, PA, USA.
24. Crawford PB, Obarzanek E, Morrison J, Sabry ZI 1994 Comparative advantage of 3-day food records over 24-hour recall and 5-day food frequency validated by observation of 9- and 10-year-old girls. J Am Diet Assoc **94:**626–630.
25. O'Connor J, Ball EJ, Steinbeck KS, Davies PSW, Wishart C, Gaskin KJ, Baur LA 2001 Comparison of total energy expenditure and energy intake in children aged 6-9 y. Am J Clin Nutr **74:**643–649.
26. Laib A, Hilderbrand T, Hauselmann HJ, Ruegsegger P 1997 Ridge number density: A parameter for in vivo bone structure analysis. Bone **21:**541–546.
27. Laib A, Hauselmann HJ, Ruegsegger P 1998 In vivo high resolution 3D-QCT of the human forearm. Technol Health Care **6:**329–337.
28. Parfitt AM 1983 Stereologic basis of bone histomorphometry: Theory of quantitative microscopy and reconstruction of the third dimension. In: Recker RR (ed.) Bone Histomorphometry: Techniques and Interpretation. CRC Press, Boca Raton, FL, USA, pp. 53–87.
29. van Lenthe GH, Muller R 2006 Prediction of failure load using micro-finite element analysis models: Toward in vivo strength assessment. Drug Discov Today: Technol **3:**221–229.
30. Melton LJ III, Riggs BL, van Lenthe GH, Achenbach SJ, Muller R, Bouxsein M, Amin S, Atkinson EJ, Khosla S 2007 Contributions of in vivo structural measurements and load/strength ratios to the determination of forearm fracture risk in postmenopausal women. J Bone Miner Res **22:**1442–1448.
31. Arbenz P, van Lenthe GH, Mennel U, Muller R, Sala M 2008 A scalable multi-level preconditioner for matrix-free micro-finite element analysis of human bone structures. Int J Numer Methods Eng **73:**927–947.
32. Chiu J, Robinovitch SN 1998 Prediction of upper extremity impact forces during falls on the outstretched hand. J Biomech **31:**1169–1176.
33. Khosla S, Amin S, Singh RJ, Atkinson EJ, Melton LJI, Riggs BL 2008 Comparison of sex steroid measurements in men by immunoassay versus mass spectroscopy and relationships with cortical and trabecular volumetric bone mineral density. Osteoporos Int **19:**1465–1471.
34. Parfitt AM 1994 The two faces of growth: Benefits and risks to bone integrity. Osteoporos Int **4:**382–398.
35. Smith EP, Boyd J, Frank GR, Takahashi H, Cohen RM, Specker B, Williams TC, Lubahn DB, Korach KS 1994 Estrogen resistance caused by a mutation in the estrogen-receptor gene in a man. N Engl J Med **331:**1056–1061.
36. Carani C, Qin K, Simoni M, Faustini-Fustini M, Serpente S, Boyd J, Korach KS, Simpson ER 1997 Effect of testosterone and estradiol in a man with aromatase deficiency. N Engl J Med **337:**91–95.
37. Bilezikian JP, Morishima A, Bell J, Grumbach MM 1998 Increased bone mass as a result of estrogen therapy in a man with aromatase deficiency. N Engl J Med **339:**599–603.
38. Rochira V, Faustini-Fustini M, Balestrieri A, Carani C 2000 Estrogen replacement therapy in a man with congenital aromatase deficiency: Effects of different doses of transdermal estradiol on bone mineral density and hormonal parameters. J Clin Endocrinol Metab **85:**1841–1845.
39. Bouillon R, Bex M, Vanderschueren D, Boonen S 2004 Estrogens are essential for male pubertal periosteal bone expansion. J Clin Endocrinol Metab **89:**6025–6029.
40. Gilsanz V, Gibbens DT, Roe TF, Carlson M, Senac MO, Boechat MI, Huang HK, Schulz EE, Libanati CR, Cann CC 1988 Vertebral bone density in children: Effect of puberty. Radiology **166:**847–850.
41. Gilsanz V, Roe TF, Mora S, Costin G, Goodman WG 1991 Changes in vertebral bone density in black girls and white girls during childhood and puberty. N Engl J Med **325:**1597–1600.
42. Gilsanz V, Skaggs DL, Kovanlikaya A, Sayre J, Loro ML, Kaufman F, Korenman SG 1998 Differential effect of race on the axial and appendicular skeletons of children. J Clin Endocrinol Metab **83:**1420–1427.
43. Muller ME, Webber CE, Bouxsein ML 2003 Predicting the failure load of the distal radius. Osteoporos Int **14:**345–352.
44. Boutroy S, Van Rietbergen B, Sornay-Rendu E, Munoz F, Bouxsein ML, Delmas P 2008 Finite element analysis based on in vivo HR-pQCT images of the distal radius is associated with wrist fracture in postmenopausal women. J Bone Miner Res **23:**392–399.
45. Aaron JE, Makins NB, Sagreiya K 1987 The microanatomy of trabecular bone loss in normal aging men and women. Clin Orthop Relat Res **215:**260–271.

Received in original form October 2, 2008; revised form November 10, 2008; accepted December 22, 2008.